Journal of Physical Sciences, Vol. 14, 2010, 207-218
ISSN: 0972-8791, www.vidyasagar.ac.in/journal
Published on December 24, 2010

Direct Current Electrical Transport and Magneto Transport Properties of Polyaniline Nanocomposites

G. Chakraborty[1], K. Gupta[1], A. K. Meikap[1] and P. C. Jana[2]

[1]Department of Physics, National Institute of Technology, Durgapur
Mahatma Gandhi Avenue, Durgapur – 713 209, West Bengal, India
Email: meikapnitd@yahoo.com

[2]Department of Physics and Technophysics, Vidyasagar University,
Midnapore- 721102, West Bengal, India.
Email: pareshjana@rediffmail.com

Received November 05, 2010; accepted November 30, 2010

ABSTRACT

Polyaniline nanocomposites were prepared by in-situ polymerization with hydrochloric acid (HCl), Copper Chloride ($CuCl_2$) and multiwall Carbon Nanotube (MWCNT). The samples were characterized by X-ray diffraction (XRD), Scanning electron microscope (SEM). Direct current electrical conductivity was measured within a temperature range $77 \leq T \leq 300$K in presence and in absence of a magnetic field up to 1Tesla. The dc transport properties of the samples follow the variable range hopping (VRH) theory. The magnetoconductivity of the samples have been explained by wave function shrinkage model and forward interference model.

Keywords: Polyaniline, Copper Chloride, Multi walled Carbon nanotubes, Charge transport, Conductivity, Magnetoconductivity

1. Introduction

The widespread application of conducting polymers in different prospects such as solar cell, schottkey junctions, electromagnetic interference shielding, batteries, sensors and microelectronics has increased their importance during the last few decades [1-3]. Polyaniline (PANI) is one of the most promising materials among these conducting polymers having good chemical and thermal stability, easy polymerizing property, solubility and dopability for the studies of electron transport phenomenon. The experimental observation has revealed the fact that, the electrical conductivity of PANI can be enhanced by several orders of magnitude by incorporating conductive fillers. On the other hand, carbon nanotubes have a vast application in electronic devices [4-5] and nanocomposites [6-7]. The unique

structural, mechanical, electronic and thermal properties [8] have made them attractive materials for the development of novel polymer-nanocomposite materials with increased functionality, such as enhanced conductivity, thermal stability and reinforcement properties [9-11].

Synthesis and characterization of PANI doped with HCl, MWNT and Copper Chloride respectively is reported in this article. In order to show the effects of MWNT and $CuCl_2$ on the conductivity and magnetoconductivity of PANI, the detailed electrical transport properties such as dc conductivity and magnetoconductivity the samples are investigated in the temperature range 77-300K in presence and in absence of a magnetic field up to 1T.

2. Sample Preparation and Experimental Techniques

2.1 Materials: Aniline, MWNT (Nanocyl 3100), copper chloride, Hydrochloric acid, ammonium peroxodisulphate (APS), cetyltrimethylammonium bromide (CTAB), ethanol and acetone are used as received from the market and purified them as required for this investigation. Aniline is double distilled under vacuum.

2.2 Synthesis: PANI-MWNT composite is prepared by in situ chemical oxidative polymerization in presence of cationic surfactant CTAB. In a typical synthesis process, 1.136 gm CTAB and 60 mg MWNT are poured in 300 ml 1(M) HCl solutions and ultrasonicated till a well-dispersed suspension is obtained. The suspension is then cooled down to 1-5^{o}C in the refrigerator. A precooled solution of 1.2 gm (1.2 ml) aniline monomer and 125 ml 1(M) HCl containing 2.72 gm APS are added sequentially to the above suspensions. The reaction mixture is stirred for 30 minutes at ice chamber and then left standing in the refrigerator at 1-5^{o}C for 24 hr. After that, the resulting black precipitate is filtered and washed with distilled water, acetone and methanol several times, and finally dried at room temperature in a dynamic vacuum for 24 hr. To prepare PANI-HCl and PANI-$CuCl_2$ composite we have taken acidified (1 M HCl) 1 mM aniline solution in a round bottom flask placed in an ice bath and 5 mM $CuCl_2$ solution is added to it. After 30 minutes of mixing, a precooled 1 M APS solution is added slowly for 30 minutes to the above mixture. A light green solution is obtained which indicates the formation of polyaniline. This solution is kept at stirring for another 24 hours to complete the polymerization process and then the solution is centrifuged at 10000 rpm for an hour. The solid mass obtained is washed and dried similarly. A PANI-HCl composite is prepared similarly without using $CuCl_2$ solution for comparison purposes. The PANI-HCl sample has been marked as S_0, PANI-MWCNT as S_1 and PANI-$CuCl_2$ as S_2 respectively.

2.3 Characterization: The X-ray diffraction (XRD) pattern was recorded using X Pert pro X-ray diffractometer (PANLYTICAL) with nickel filter Cu k_α radiation (λ=1.5414 Å) in 2θ range from 20 to 70^{0}. Scanning electron microscopy (SEM) was used to study morphology of PANI composites. SEM was conducted at 15 KV using and electronic diffraction images were recorded in HITACHI (S-300N) instrument and electronic diffraction images were recorded. The electrical conductivity of the

samples was measured by a standard four probe method after good contact was ensured with highly conducting graphite adhesive (Electrodag 5513, Acheson, Williston, VT) and fine copper wires as the connecting wires. The dc conductivity was measured with an $8^1/_2$ – digit Agilent 3458A multimeter. The temperature dependence of the conductivity was studied with a liquid nitrogen cryostat. For the control and measurement of the temperature, an ITC 502S Oxford temperature controller was used. To measure the dc response, pellets of 1 cm in diameter of the samples was made by pressing the powder under a hydraulic pressure of 500 MPa. The magnetoconductivity was measured in the same manner by the variation of the transverse magnetic field (B<1T) with an electromagnet.

3.1 Results and discussion

3.1 Morphology:

Figure 1(a) shows the scanning electron micrograph of PANI-MWNT. It is observed from the micrograph of PANI-MWNT that carbon nanotubes are arranged parallel and polymer chains are also aligned along it around the MWNT. Figure 1(b) shows the scanning electron micrograph of PANI-$CuCl_2$ and it also composed of rod like structures having an average diameter of 70-90 nm. The length of the rods is ~ 2-3 micrometers. Copper chlorides may be present inside the polyaniline nanorods or within the rod bunches.

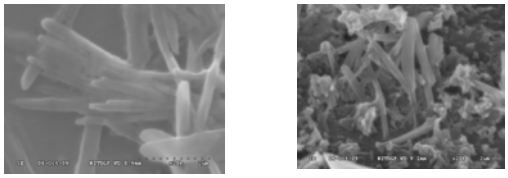

Figure 1 SEM micrograph of PANI-MWNT and PANI-$CuCl_2$

3.2 Structural characterization:

XRD of PANI and its composite with MWNT and $CuCl_2$ are shown in figure 2. It is observed from the XRD pattern that PANI exhibit two broad peaks at $2\theta = 14.9°$ and 25.1°, which may arise due to regular repetition of monomer unit aniline. The diffraction peak at $2\theta=25.1°$ indicates the densely packed phenyl rings which rise to a planar conformation. This gives an extensive interchain $\pi \rightarrow \pi^*$ orbital overlap [12-14].Therefore XRD pattern confirms the formation of PANI. PANI-$CuCl_2$ shows monoclinic crystalline structure (Joint Committee on Powder Diffraction Standards No 79-1635). Characteristic peaks obtained in the spectrum are at 2θ = 30.61, 37.90, 50.10, 53.19, and 64.15 degree. Reflecting planes of the corresponding peaks are $200, \bar{1}12$, 112, $\bar{3}13$ and $\bar{1}14$. These observed peaks are of copper chloride ($CuCl_2$). Therefore XRD analysis confirms the presence of copper chloride in the polyaniline matrix. MWNTs are introduced in the polyaniline matrix, the peaks of PANI and MWNT coincide. As a result, the XRD pattern is much sharper and peak broadening has occurred.

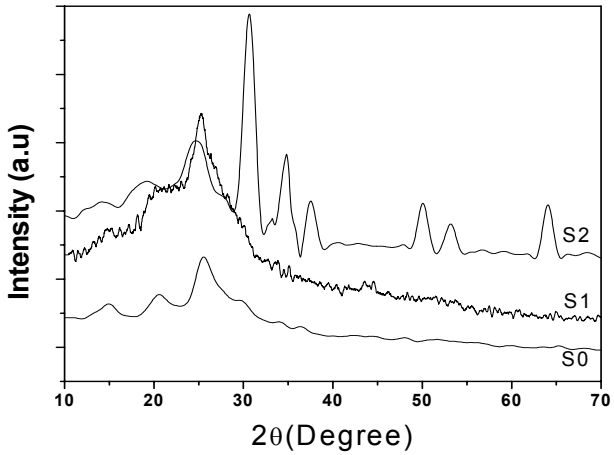

Figure 2 XRD pattern

3.3 DC Conductivity: To have a clear understanding of the electrical transport properties of the samples, the dc resistivity of the specimens have been measured within a temperature range of $77 \leq T \leq 300K$. The room temperature resistivity of S0 is $4.7 \times 10^{3} \Omega$-m whereas it is of the order of 1.73 Ω-m and 1.59×10^{-2} Ω-m in case of S1 and S2 respectively. Thus, the incorporation of MWNT and $CuCl_2$ in PANI matrix may be the reason behind this increased conductivity. MWNTs are considered as a good electron acceptors whereas PANI are the good electron donors. The interaction of the quinoid ring of the PANI and the MWNT facilitate the charge transfer processes between the two components. The localization length (L_{loc}) of MWNT is around 10nm due to its large π-conjugated structure and the localization length of crystalline or amorphous PANI is only 2nm [15]. So the strong coupling between the poorly conducting polymer and highly conducting MWNTs enhances of the average localization length and hence an increase in conductivity in S1.On the other hand, presence of smaller amount of Cu in S2 causes the formation of metallic islands of smaller sizes in between the insulating matrices resulting in the localization of the electronic wave functions in smaller regions and localization length of smaller dimensions. Thus, for a significant number of Cu atoms for a larger concentration of $CuCl_2$ in PANI matrix, there is an enlargement of metallic island in S_2 and the three dimensional (3D) coupling through the more rod-like chains between metallic island induce the 3D coupled mesoscopic metallic region to be formed in S_2 at high temperature enhances its

conductivity [16]. In general, the conductivity of the material depends on the content of disorder present in the samples that is measured in terms of the resistivity ratio ρ_r[ρ(77K)/ ρ(300K)].It is observed from the conductivity study, that the values of ρ_r are 12.08 in S_0, 8.77 in S_2 and 2.25 in S_1 respectively. Clearly, the large value of resistivity ratio in S_0 sample indicates the presence of more disorder than the other two samples for which the conductivity of the other two samples is greater than S_0. All the samples have shown semiconducting behavior i.e., their resistivity decreases with increasing temperature. It happens due to the increase in charge transfer process between the polymer and the dopants like MWNT and Cu with increasing temperature. In general, the temperature variation of the disordered semiconducting samples can be explained by Mott's variable range hopping theory. According to this theory [17], the resistivity is given by

$$\rho(T) = \rho_0 \exp\left(\frac{T_{Mott}}{T}\right)^{\gamma} \quad (1)$$

where γ is the VRH exponent, whose value determines the dimension of the conducting system by the relation $\gamma = 1/(1+d)$. The value of γ is 1/4 for three dimensional system, 1/3 for two dimensional system and 1/2 for one dimensional system respectively. ρ_0 is the resistivity at infinite temperature, T_{Mott} is the Mott Characteristic temperature, which usually depends on the hopping barrier, electronic structure and the energy distribution of the localized states can be expressed as

$$T_{Mott} = \frac{24}{\pi k_B N(E_F) L_{loc}^3} \quad (2)$$

where k_B is the Boltzmann Constant, $N(E_F)$ and L_{loc} are the density of states at the Fermi level and localization length respectively. To investigate the charge transfer mechanism in detail, a graph of ln[ρ(T)] with $T^{-1/4}$ have been plotted and shown in figure 3. The resistivity of all the samples vary non- linearly in the low temperature range but shows a linear variation at the higher temperature. To explain the nature of temperature variation of resistivity, two different slopes have been drawn for all the samples. At the low temperature region 77≤T≤120K, slopes have lower value and at high temperature region 120≤T≤3000K the slopes have larger values but in both region, the experimental data are in accordance with the theoretical curve obtained from eqn.(1). Therefore, the linear variation of ln[ρ(T)] with $T^{-1/4}$ indicates that the three dimensional (3D) charge transport (γ = ¼)mechanism occurs in the investigated sample. The values of T_{Mott} in both the temperature regions have been calculated from the slopes of the linear variation of ln[ρ(T)] with $T^{-1/4}$and are indicated in table-1. The values of T_{Mott} varies from 162.46K to 13882.76K in the lower temperature region (77-120K) and in the higher temperature region (120-

300K), it varies in between 1.17 x10^4 K to 1.59 x 10^6 K. In our present investigation, the experimental data support the three dimensional VRH model. When the conducting polymer chains are not isolated due to the presence of the conducting islands between the insulating matrices, the electronic wave function gets extended three dimensionally. S2 may be composed of parallel chains that form metallic bundles in which the electron wave function gets extended three dimensionally. So, 3D-VRH is the dominating charge transport mechanism of the investigated samples which is supported by the experimental data. At the lower temperature region (77≤T≤120K), the dominant conduction mechanism through the polymer chains may be the reason behind the observed nonlinearity in the graph of ln[ρ(T)] with $T^{-1/4}$ for the investigated samples.

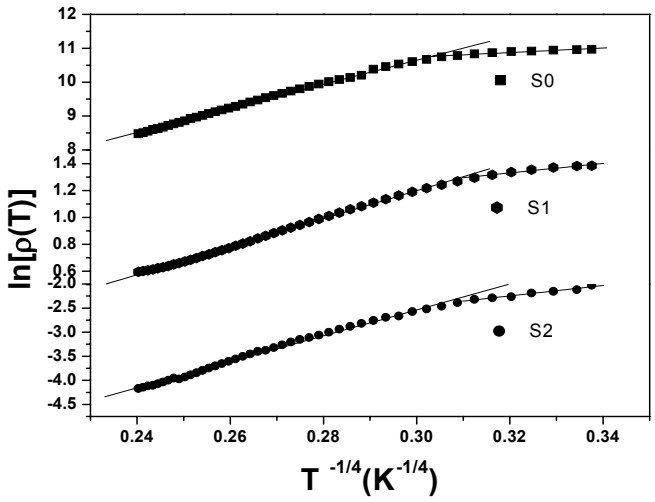

Figure 3 Temperature dependence of dc resistivity of different PANI composites. The solid lines are fitted to eqn.(1).

In order to obtain clear understanding, the activation behavior of all the samples have been studied by the Arrhenius relation

$$\rho(T) = \rho_0 \exp(\frac{E_a}{k_B T}) \quad (3)$$

where Ea is the activation energy of the investigated sample. Figure 4 shows a plot of ln [ρ(T)] with 1000/T for all the samples. The resistivity all the samples vary nonlinearly indicating the presence different activation energy. From the slopes of the straight line variation in the two regions, the activation energy of different samples has been calculated. The estimated values of E_a are indicated in table-1. In

the temperature range 77≤T≤120K , the values of Ea are 4.99meV for S0, 4.36 meV for S2 and 2.79 meV for S1 respectively whereas in the higher temperature range120≤T≤3000K , the value of Ea are 39.49 meV for S0 , 34.08 meV for S2 and 11.18 meV for S1 respectively. The interaction of PANI with MWNT and $CuCl_2$ increases at higher temperature than at lower temperatures which results a larger Ea at higher temperature. As a result, a non linear variation of resistivity with temperature occurs for all the samples that is observed in figure 3. So, it may be concluded that, at higher temperature, the charge transport is dominated by the MWNT and Cu atom than in the lower temperature region.

3.4 DC Magnetoconductivity: The magnetoconductivity of the different samples has been measured within a temperature range 77 ≤ T ≤ 300K under the influence of a varying magnetic field up to 1 Tesla. Figure 5 shows the variation of magnetoconductivity with magnetic field strength at room T=100K.The samples S_0 and S_2 shows positive magnetoconductivity but the sample S_1 shows negative magnetoconductivity.

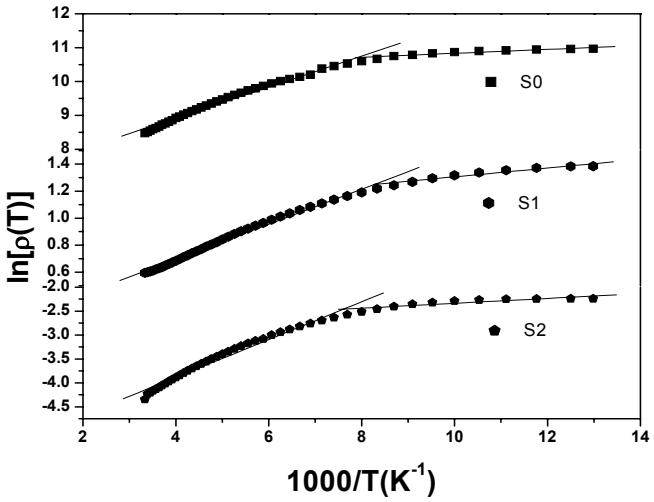

Figure 4 Variation of dc resistivity with temperature of different PANI composites. The solid lines are fitted to eqn.(3).

The maximum percentage change of conductivity $\left[\frac{\sigma(B,T)-\sigma(0,T)}{\sigma(0,T)}X100\right]$ in the presence of magnetic field 0.8T at 300K is about -6.24 % for S0, -0.36% for S1 and -1.13% for S2 respectively. The magnetic response of the samples can be explained in terms of two simultaneously acting hopping processes, wave function shrinkage model [18-19] and the forward interference model (orbital magnetoresistivity) [20-22]. According to the wave function shrinkage model, the wave functions of the

electrons reduce upon increasing magnetic field. As a consequence; there is a reduction of the wave functions of the electrons and hence decrease in the average hopping length resulting in negative magnetoconductivity i.e. the wave function shrinkage model can predict the decrease in conductivity with increasing magnetic field. In this theoretical model, the magnetoconductivity ratio under a small magnetic field can be expressed as

$$\ln\left(\frac{\sigma(B,T)}{\sigma(0,T)}\right) = -t_1 \frac{e^2 L_{loc}^4}{\hbar^2}\left(\frac{T_{Mott}}{T}\right)^{3/4} B^2 \qquad (4)$$

where, $t_1 = 5/2016$ and L_{loc} is the localization length. On the other hand, the forward interference model (quantum interference model) predicts the effect of forward interference among random paths in the hopping process between two sites spaced at a distance equal to the optimum hopping distance and this theory predicts the positive magnetoconductivity. According to this model, the magnetoconductivity ratio can be expressed as:

$$\frac{\sigma(B,T)}{\sigma(0,T)} = 1 + \frac{\frac{C_{sat}B}{B_{sat}}}{1+\frac{B}{B_{sat}}} \qquad (5)$$

where C_{sat} is a temperature independent parameter and $B_{sat} = 0.7(h/e)(8/3)^{3/2}(1/L_{loc}^2)(T/T_{Mott})^{3/8}$. Figure 5 shows that the experimental data is in accordance with the theoretical models. Due to the small localization length (L_{loc}) of PANI, the average hopping length (R_{hopp}) of it becomes smaller. So, many previous studies reported that the wave function shrinkage model is found to follow by PANI [23-24] Again, MWNT films and pellets show a large positive magnetoconductivity for its large L_{loc} and R_{hopp}. [25-26].Such behavior of MWNT can be interpreted in terms of quantum interference effect. Therefore, in S_1, there is a competition between these two opposite behavior and hence there is a change in sign and magnitude of magnetoconductivity. At lower temperature, both S_0 and S_1 show positive magnetoconductivity which can be interpreted in terms of forward interference model. The positive magnetoconductivity provides a strong evidence to support the larger average localization length of the S_0 and S_2 samples at lower temperature.

Figure 6 shows the variation of magnetoconductivity of S_2 sample with magnetic field at different temperatures. The magnetoconductivity changes sign from positive to negative upon increasing the temperature. The magnitude of the magnetoconductivity decreases with increasing temperature and ultimately becomes negative at a temperature T = 300K due to the decrease of average hopping length. In figure 6 the points represent the experimental data while the solid lines are the best fits obtained from equation (5) for temperature T = 77K, 100K, 150K , 200K and 250K respectively and from equation (4) for T = 300K. It is evident from the figure 6 that the experimental data can be well explained by above theories. At lower

temperature, the positive magnetoconductivity of S2 can be explained by the quantum interference effect but as the conductivity decreases at higher temperature, it may be considered that the wave function shrinkage effect dominates over the quantum interference effect and ultimately at T=300K the conductivity becomes negative.

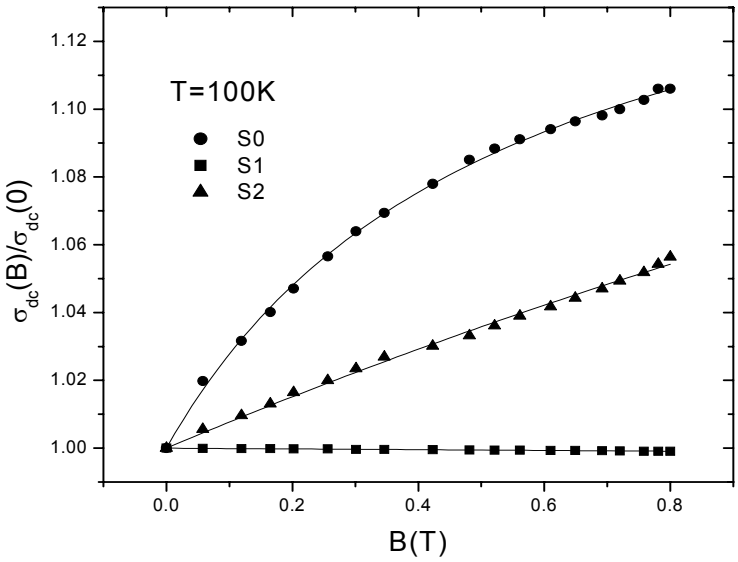

Figure 5 Variation of the dc magnetoconductivity with perpendicular magnetic field of different samples at 100K. The solid lines are fitted to Eq.(4) for S_1 and Eq.(5) for S_0 and S_1.

Table-1 Different physical parameters of samples: Conductivity at room temperature (ρ (300K)), resistivity ratio (ρ_r), temperature exponent (γ), Mott characteristic temperature in the temperature range $77 \leq T \leq 120K$(T_{Mott}), Mott characteristic temperature in the temperature range $120 \leq T \leq 3000K$ (T_{Mott}), Activation energy(Ea) in the temperature range $77 \leq T \leq 120K$, Activation energy(Ea) in the temperature range $120 \leq T \leq 300K$,Percentage change in magnetoconductivity

Parameters	**S0**	**S1**	**S2**
ρ(300K) (Ω-m)	4.79×10^{3}	1.73	1.59×10^{-2}

ρ_r	12.08	2.256	8.77
γ	0.25	0.25	0.25
(T_{Mott}) (K) at $77 \leq T \leq 120K$	2006.34	162.46	13882.76
(T_{Mott}) (K) at $120 \leq T \leq 3000K$	1.59×10^6	1.17×10^4	5.28×10^5
E_a (meV) at $77 \leq T \leq 120K$	0.175	0.156	0.211
E_a (meV) at $120 \leq T \leq 300K$	1.17×10^6	2.06×10^4	6.13×10^5
$\frac{\sigma(B,T)-\sigma(0,T)}{\sigma(0,T)} X100$	-6.24	-0.36	-1.13

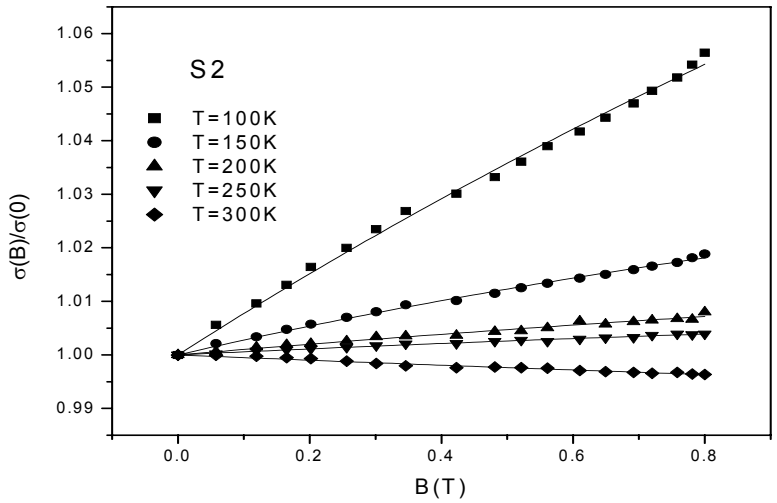

Figure 6 Variation of the dc magnetoconductivity with perpendicular magnetic field of S_2 at different temperatures. The solid lines are fitted to Eq.(4) for T = 300K and to Eq.(5) for T = 77K, 100K,150K , 200K and 250K.

4. Conclusions

The electrical conductivity of the investigated samples has been measured in the absence and also in the presence of the perpendicular magnetic fields. The room temperature conductivity $\sigma(300K)$ increases by introducing the highly conducting MWNT and Cu atoms in insulating polymer matrix. The maximum conductivity was obtained for the sample S_2 due to the presence of small metallic islands inside the polymer matrix. Three dimensional VRH charge transport is observed in all the samples. The non linear temperature variation of resistivity can be interpreted in terms of two different activation energies of the samples. The positive magnetoconductivity of S0 and S2 follows forward interference model while S1 follows wave function shrinkage model. Sample S2 shows a change in magnetoconductivity from positive to negative upon increasing the temperature due to the possible dominance of wave function shrinkage effect over quantum interference effect.

Acknowledgements

The authors gratefully acknowledge the principal assistance received from the MHRD, Government of India during this work. Authors are also thankful to the department of Physics and Technophysics, Vidyasagar University, Midnapore for allowing us to use the instrumental facilities.

REFERENCES

1. J. H. Burroughes, D C Bradely, A R Brown, R N marks, K Mackey, R H Friend and P L Bruns Nature 347, 539 ,1990.
2. A. G. Mac Diarmid Conjugated Polymers and Relater Materials (London, Oxford University), 1993.
3. H. Naarmann Science and Application of Conducting Polymers (Bristol, Adam Hilger), 1991.
4. J Sandler, M S P Shaffer, T Prasse, W Bauhofer, K Schulte, A N Windle Polymer 40, 5967, 1999
5. A B Dalton, S Collins, E Munoz, J M Razal, V H Ebron, J P Ferraries et al Nature 423, 703, 2003.
6. S Fan, M G Chapline, N R Franklin, T W Tombler, A M Cassell, H Dai Science 283, 512, 1999.
7. A Modi, N Koratkar, E Lass, B Wei, P M Ajayan Nature 424, 171, 2003.
8. C N R Rao, B C Satishkumar, A Govindaraj, M Nath Chem. Phys. Chem. 2, 78, 2001.
9. S A Curran, P M Ajayan, W J Blau, D L Carroll, J N Coleman, A B Dalton, A P Davey, A Drury, B Mccarthy, S Maier, A Strevens Adv. Mater 10, 1091,1998.

10. M Cochet, W K Maser, A M Benito, M A Callejas, M T Martinez, J M Benoit, J Schreiber, O Chauvet Chem. Comm. 1450,2001.
11. H Zengin, W Zhou, J Jin, R Czerw, Jr D W Smith, L Echegoyen, D L Carroll, S H Foulger, J Ballato Adv. Mater 14, 1480, 2002
12. J. Stejskal, A. Riede, D. Hlavata, J. Prokes, M. Helmstedt, P. Holler, Synth. Met. 96, 55, 1998
13. M. Trchova, I. Sedenkova, E.N.Konyushenko, J. Stejskal, P. Holler, G. Gric-Marjanovic, J. Phys. Chem. B 110, 9461, 2006
14. A. Dey, S. De, A. De , S. K. De, Nanotechnology 15, 1277, 2004
15. J. Joo, S. M. Long, J. P. Pouget, E. J.Oh, A. G MacDiarmid, A. J. Epstein, Phys Rev B 57, 9567, 1998.
16. J. Joo, Z. Oblakowski, G. Du, J. P. Pouget, E. J. Oh, J. M. Wiesinger, Y. Min, A. G. MacDiarmid and A. J. Epstein Phys. Rev. B 49 2977, 1994.
17. N. F. Mott and E. A. Davis Electronic Processes in Non Crystalline Materials, 2nd Ed. (Oxford, Clarendon Press), 1979
18. B. I. Shklovskii, Sov Phys Semicond 17, 1311, 1983.
19. B. I. Shklovskii, A. L. Efros, Electronic Properties of Doped Semiconductors; Springer: Berlin, p 202, 1984.
20. V. L. Nguyen, B. Z. Spivak, B. I. Shklovskii, Sov Phys JETP 62, 1021,1995.
21. U. Sivan, O. Entin-Wohiman, Y. Imry, Phys Rev Lett 60, 1566, 1988.
22. R. Rosenbaum, A. Milner, S. Hannens, T. Murphy, E. Palm, B. Brandt, Phys B 294–295, 340, 2001.
23. M. Ghosh, A. Barman, A. K. Meikap, S. K.De, S. Chatterjee, Phys Lett A 260, 138, 1999.
24. P. Ghosh, A.Sarkar, A. K. Meikap, S. K. Chattopadhyay, S. K. Chatterjee, M. Ghosh, J Phys D: Appl Phys 39, 3047, 2006.
25. M. S. Fuhrer, W. Holmes, P. L. Richards, P. Delaney, S. G. Louie, A. Zettl, Synth Met 103, 2529, 1999.
26. Y. Yosida, I. Oguro, J Appl Phys 86, 999, 1999.